metals

MDPI

Article

Evolution of Inclusions and Cleanliness in Ti-Bearing IF Steel Produced via the BOF–LF–RH–CC Process

Baohui Yuan [1], Jianhua Liu [1,*], Jianhua Zeng [2], Min Zhang [2], Jihong Huang [3] and Xiaodong Yang [1,3]

[1] National Engineering Research Center for Advanced Rolling and Intelligent Manufacturing, University of Science and Technology Beijing, Beijing 100083, China; yuanbaohui20@163.com (B.Y.); xiaodong2984@163.com (X.Y.)
[2] Pangang Group Research Institute Co., Ltd., Panzhihua 617000, China; yjyzjh@126.com (J.Z.); muyufile@163.com (M.Z.)
[3] Pangang Group Xichang Steel and Vanadium Co., Ltd., Xichang 615032, China; huangjihong2022@163.com
* Correspondence: liujianhua@metall.ustb.edu.cn

Abstract: Owing to the insufficient converter heat, IF steel is produced via the BOF–LF–RH–CC process in Pangang Group Xichang Steel and Vanadium Co., Ltd. To clarify the evolution of inclusions and the control strategy to improve the cleanliness of molten steel in Ti-bearing IF steel produced via the long process, scanning electron microscopy with energy spectroscopy analysis and automatic scanning electron microscopy were employed to analyze the number, size, type and morphology of inclusions in IF steel from RH to tundish. The results show that the characteristics of inclusions are similar in two heats during RH treatment. In the tundish sample of Heat 2, the number density (ND) and area fraction (AF) of Al_2O_3 and $Al_2O_3{\cdot}TiO_x$ inclusions increase significantly, and the size of Al_2O_3 inclusions decreases obviously, which is closely related to the serious reoxidation of molten steel caused by the slag with high oxidability during the holding process. Meanwhile, a new method of determining the number of cluster inclusions is used to evaluate the cleanliness of IF steel in this paper, and the obtained number of inclusion clusters is consistent with the trend of ND and AF of inclusions. The effects of reoxidation on the morphology, number and other indexes of Al_2O_3 and $Al_2O_3{\cdot}TiO_x$ inclusions are discussed in detail, and there are two ways of forming $Al_2O_3{\cdot}TiO_x$ inclusions in the case of serious reoxidation. To weaken the reoxidation process and enhance the cleanliness of IF steel produced via the long process, reducing the oxygen content in molten steel before Al deoxidation, minimizing the holding time and reducing the oxidability of slag after RH are helpful.

Keywords: nonmetallic inclusion; cleanliness; Ti-bearing IF steel; reoxidation; long producing process

Citation: Yuan, B.; Liu, J.; Zeng, J.; Zhang, M.; Huang, J.; Yang, X. Evolution of Inclusions and Cleanliness in Ti-Bearing IF Steel Produced via the BOF–LF–RH–CC Process. *Metals* **2022**, *12*, 434. https://doi.org/10.3390/met12030434

Academic Editor: Mark E. Schlesinger

Received: 27 December 2021
Accepted: 21 February 2022
Published: 1 March 2022

1. Introduction

Ti-bearing IF steel is widely used in automotive, home appliances, electronics and other fields due to its good deep-drawing performance. With the market's increasing requirements for the surface and internal quality of final products, the demand for high-quality IF steel is increasing [1,2]. The performance of IF steel is greatly affected by the type, number and size distribution of nonmetallic inclusions [3–6]. Engine failure caused by nonmetallic inclusions of tens of microns is a typical problem in the automotive industry [7,8]. Clogging of the submerged entry nozzle is also a common problem in the steelmaking process because of the presence of Ti [9–12]. Therefore, it is important to enhance the potential for inclusion removal from molten steel during RH and tundish processes.

There are two routes for producing IF steel currently; one is the BOF–RH–CC short process, and the other is the BOF–LF–RH–CC long process. The short process is more universally employed in this field owing to its simpler process and better refining effect [13–17]. In Pangang Group Xichang Steel and Vanadium Co., Ltd., the hot metal after extracting vanadium with lower carbon content is smelted in BOF, resulting in the insufficient heat

of molten steel after BOF. In order to produce smoothly, electric heating (LF) is used to compensate for the heat of molten steel. Therefore, the Ti-bearing IF steel is produced via the BOF–LF–RH–CC process.

At this plant, a high oxygen activity generally in the range of 500~900 ppm after BOF is necessary to complete the deep decarburization task by the natural decarburization process during RH treatment. Due to there being no pre-deoxidation operation before RH and the longer reaction time between the molten steel and slag, the total mass fraction of the FeO and MnO in the ladle slag is basically over 15% during RH treatment. Some scholars have also studied the cleanliness control of IF steel produced via the long process [15,18,19]. However, there are few reports about the effect of the high oxidized slag on inclusions in IF steel produced via the long process, and the influence of the reoxidation process on the cleanliness of molten steel should not be ignored. In the industrial producing process, the evolution of inclusions in Ti-bearing IF steel produced by the long process also needs to be studied more deeply. Additionally, it is still not clear how to take measures to improve the cleanliness of IF steel produced via the long process.

The main objective of this work is to clarify the evolution of inclusions in the long process from RH to tundish and evaluate the influence of the reoxidation process and the relevant process parameters on the cleanliness of molten steel. Theoretical guidance obtained by these experiments is good for optimizing the long smelting process and improving the cleanliness of Ti-bearing IF steel.

2. Materials and Methods

2.1. Industrial Investigations

At the steel plant of Pangang Group Xichang Steel and Vanadium Co., Ltd., IF steel is typically produced in heat sizes of 200 tons via the basic oxygen furnace (BOF)–ladle furnace (LF)–Ruhatahl–Hausen (RH)–continuous casting (CC) process. The processes mainly include the following: (1) The BOF steelmaking is carried out after extracting vanadium. (2) The temperature of molten steel is increased in LF. (3) After ending the decarburization process, aluminum and sponge titanium are added for alloying. The interval time between the added Al and Ti is about 4 min, and the pure circulation time after Ti addition is usually around 6 min. (4) After the vacuum break, the holding time is usually between 30 and 40 min. The steps are shown in Figure 1.

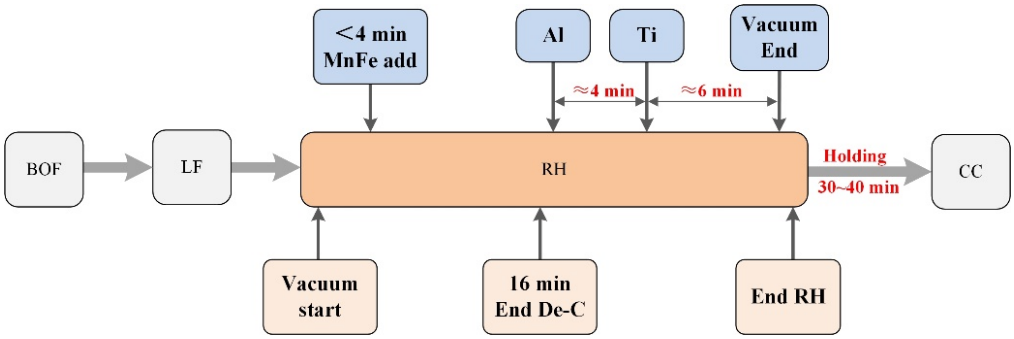

Figure 1. Steps of producing IF steel during steelmaking processes.

The inclusion landscapes of two heats have been tracked from RH to tundish, and 4 standard lollipop samples were taken in different time steps after Al addition. The exact time steps are listed in Table 1. The total oxygen (T.O) and nitrogen (N) contents of samples were analyzed using the TCH-600 oxygen/nitrogen/hydrogen analyzer (LECO Company, San Jose, CA, USA). The chemical compositions of the IF steel slab for two heats are shown in Table 2. The chemical compositions were obtained with ICP-AES (Inductively Coupled Plasma-Atomic Emission Spectrometer).

Table 1. Time of sampling and chemical composition of lollipop samples.

Sample	Heat 1			Heat 2		
	Description	T.O %	N %	Description	T.O %	N %
RH-1	2.0 min after Al addition	0.0080	0.0014	2.5 min after Al addition	0.0120	0.0011
RH-2	3.0 min after Ti addition	0.0027	0.0018	3.3 min after Ti addition	0.0052	0.0010
RH-3	6.0 min after Ti addition	0.0020	0.0018	5.0 min after Ti addition	0.0013	0.0010
Tundish	-	0.0017	0.0020	-	0.0150	0.0014

Table 2. Chemical composition of Ti-bearing IF steel (wt%).

Heats	C	Si	Mn	P	S	Al_s	Ti	N
1	0.0018	0.0030	0.1300	0.0080	0.0060	0.0250	0.0550	0.0027
2	0.0022	0.0030	0.1300	0.0060	0.0060	0.0250	0.0540	0.0018

2.2. Experimental Methods

To analyze the inclusions in the IF steel, the standard samples (15 mm × 15 mm × 15 mm) were cut from the lollipop samples. They were inlaid and ground to 2000 grit and then polished with the diamond polishing agent. The number and size distribution of nonmetallic inclusions (NMIs) were statistically analyzed by an ASPEX Explorer scanning electron microscope (FEI Company, Hillsboro, OR, USA). An area of about 83 mm^2 was set as the standard area on samples for inclusion observation, and the minimum detectable inclusion was 1.0 μm in equivalent circle diameter (ECD). The number density and area fraction are two statistical parameters to characterize the amount of nonmetallic inclusions, as shown in the following two Equations:

$$ND = \frac{n}{A_{\text{total}}} \tag{1}$$

$$AF = \frac{A_{\text{inclusion}}}{A_{\text{total}}} \tag{2}$$

where ND is the number density of inclusions, mm^{-2}; A_{total} is the sample detection area, mm^2; n is the number of detected inclusions on the area of A_{total}; AF is the area fraction of inclusions, 10^{-6}; and $A_{\text{inclusion}}$ is the total area of detected inclusions, μm^2.

A Zeiss Sigma 500 field emission scanning electron microscope (ZEISS Company, Oberkochen, Germany) was used to analyze the morphology and composition of inclusions. The inclusions in the view field of metallographic samples were observed and photographed, and energy dispersive spectroscopy (EDS) was used to determine the chemical composition of inclusions by point or plane scanning.

In the present work, the effect of relevant process parameters on the cleanliness of molten steel is further discussed. Besides Heat 1 and Heat 2, several industrial tests were carried out, and the relevant process parameters are listed in Table 3. T.Fe content is the total mass fraction of FeO and MnO in the ladle slag. The ND of inclusions in Table 3 was also analyzed by the ASPEX method and calculated by Equation (1).

Table 3. Parameters of experimental heats during RH and tundish processes.

Heats	[O] before Al Deoxidation/10^{-6}	Holding Time/Min	T.Fe in Slag after RH/%	Number Density of Inclusions/mm^{-2}	
				After RH	Tundish
1	295	35.5	15.3	13.5	9.3
2	294	42.5	18.1	15.2	35.1
3	288	35.3	14.2	9.3	6.1
4	357	26.0	17.0	15.0	2.5
5	247	32.8	16.8	2.5	13.8
6	312	34.9	9.5	9.5	4.6

3. Results and Discussion

3.1. Number and Size Distribution of Inclusions

To reveal the evolution process, the results of the ASPEX inclusion assessment for Heat 1 and Heat 2 were employed to analyze the number and size changes of inclusions from RH to tundish, as shown in Figure 2.

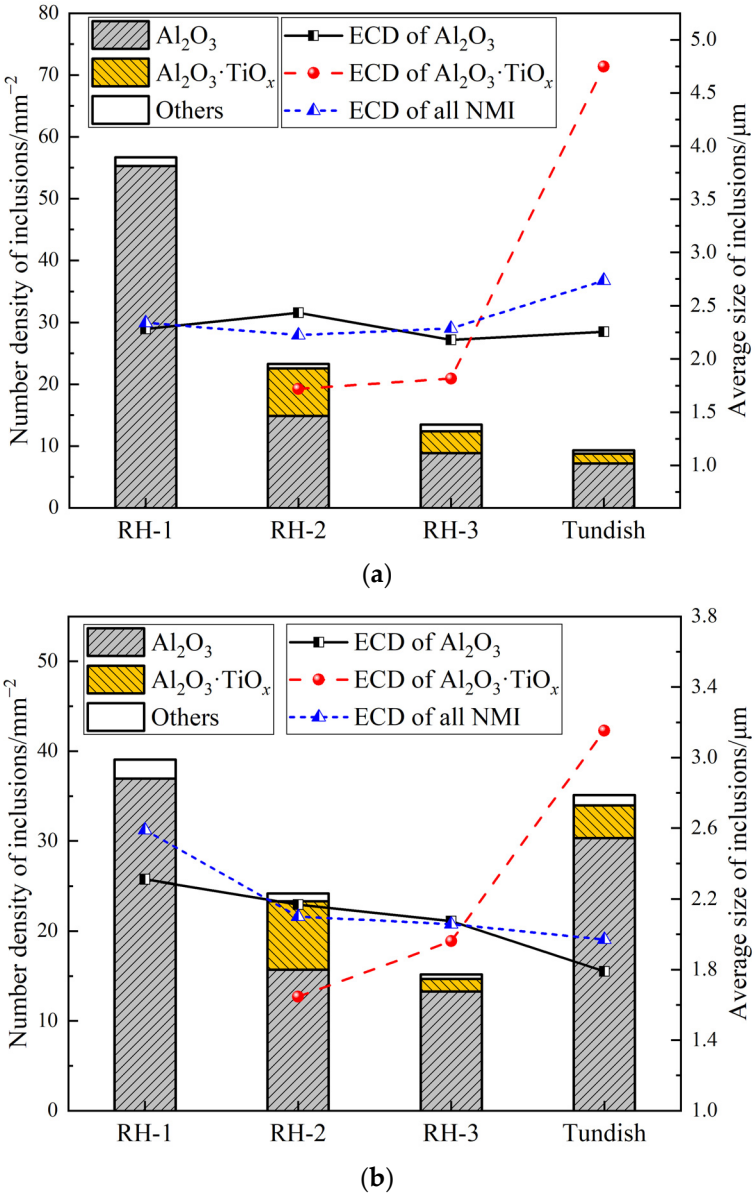

Figure 2. Number and size of different inclusions in (**a**) Heat 1 and (**b**) Heat 2 during RH treatment and tundish processes.

It can be seen from Figure 2 that inclusions in molten steel are mainly divided into three types, namely Al_2O_3, Al_2O_3·TiO_x and other inclusions. Al_2O_3 and Al_2O_3·TiO_x inclusions account for almost 100% during the whole steelmaking process. The ND of Al_2O_3 inclusions in molten steel is over 35 mm^{-2} within 3 min after Al addition, and the average size of Al_2O_3 inclusions is about 2.3 μm. The number of Al_2O_3 inclusions decreases significantly at about 3 min after Ti addition and then further decreases at the end of RH. During the whole RH refining process, the size of Al_2O_3 inclusions changes a little. After adding the sponge titanium, the formation of many small Al_2O_3·TiO_x inclusions causes the reduced size of all NMIs, and the size of Al_2O_3·TiO_x inclusions in the pure circulation process shows a growing trend. In the tundish sample of Heat 1, the mean size of all inclusions increases

to about 2.7 μm owing to the notable increasing size of $Al_2O_3 \cdot TiO_x$ inclusions. On the contrary to Heat 1, the number of various inclusions in the tundish sample of Heat 2 has an increasing trend. In particular, the number of Al_2O_3 inclusions in tundish is more than twice as much as that at the end of RH. The mean size of all inclusions shows a decreasing trend, which is also related to the increase in small Al_2O_3 inclusions.

Figure 3 shows the change of the AF of inclusions during RH treatment and tundish processes. In Figure 3, the AF of inclusions shows basically the same trend with the ND of inclusions. In the tundish sample of Heat 2, the AF of Al_2O_3 and $Al_2O_3 \cdot TiO_x$ inclusions also increases significantly. The process characteristics for producing IF steel in this steel plant are the main reason for this phenomenon.

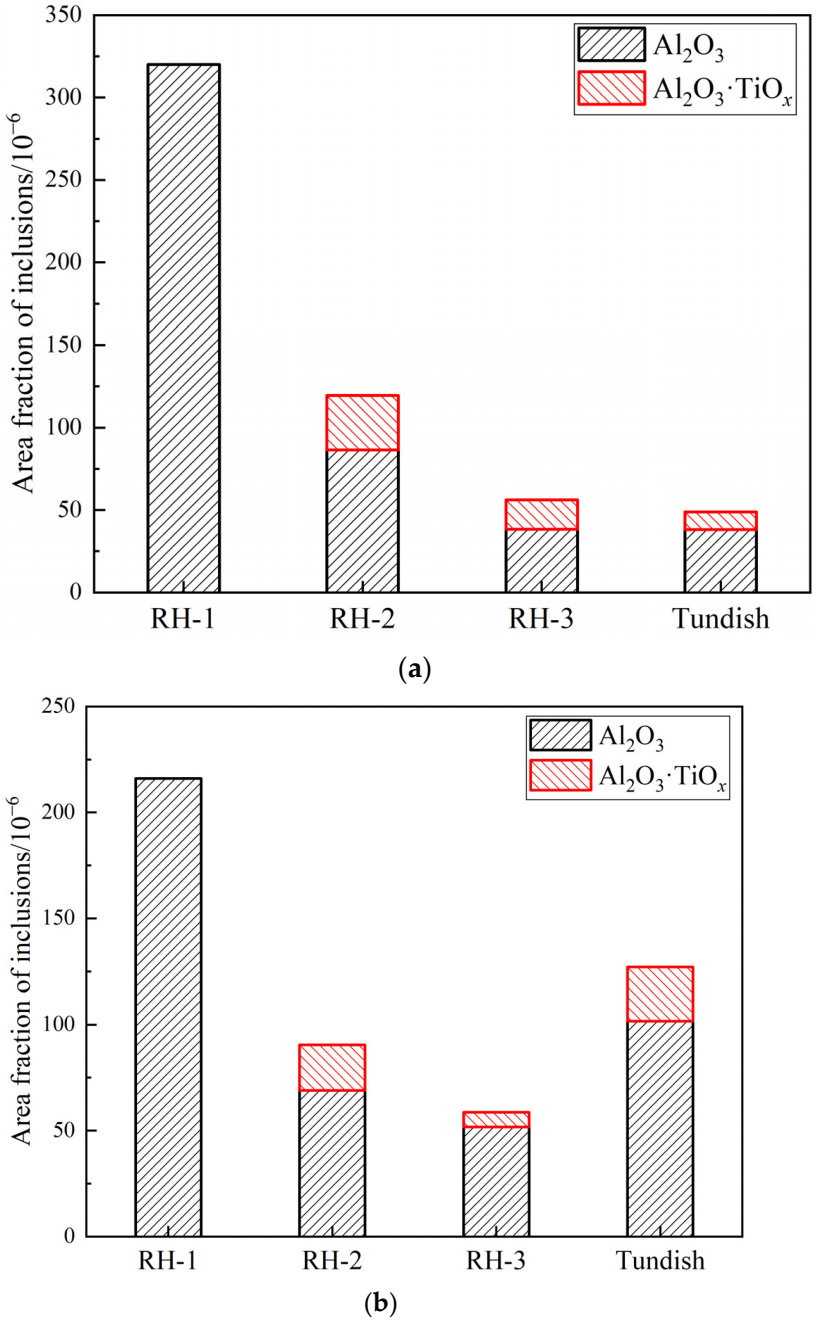

Figure 3. Change of the area fraction of inclusions in (**a**) Heat 1 and (**b**) Heat 2 during RH treatment and tundish processes.

IF steel in this plant is produced via the BOF–LF–RH–CC process, and the molten steel is in a state of peroxidation at the end of BOF. The oxygen in molten steel is continuously transferred to the ladle slag, resulting in the near-equilibrium conditions at the steel/slag interface. Moreover, no pre-deoxidation measures are taken before the RH refining. Consequently, the ladle slag oxidability is still at a high level despite taking the slag denaturalization treatment, and the T.Fe content in the ladle slag after RH is basically over 15%. Figure 4 shows the mean Ti percentage through the arithmetic average of Ti-containing inclusions. In this figure, the mean Ti percentage in Ti-containing inclusions increases gradually, especially more greatly from RH-end to tundish. It indicates that the reoxidation of molten steel occurs during the holding process. Simultaneously, the inclusion amount and the T.O content in molten steel for Heat 2 have a large increase in the tundish sample, indicating that the reoxidation is relatively serious under the actual producing conditions in this plant.

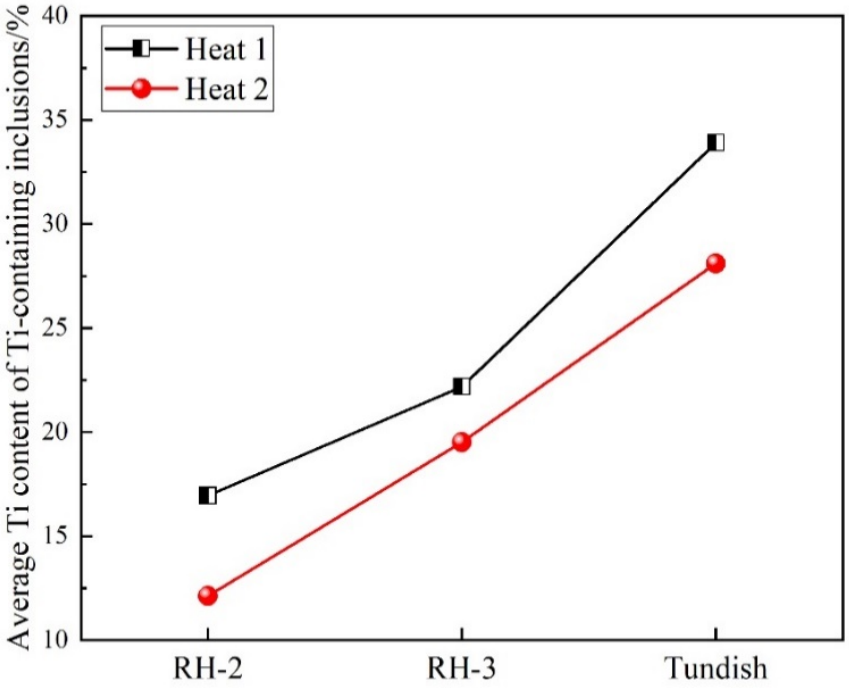

Figure 4. Transformation of inclusion composition during RH refining and tundish processes.

The unstable oxides in slag or refractory materials, including FeO, MnO, SiO_2 and other oxides; a source of oxygen in the added Ti-Fe alloy or sponge titanium; and the air inhalation into molten steel under the poor protection effect may all cause the reoxidation of molten steel, resulting in the increased content of the dissolved oxygen and total oxygen and a large loss of alloying elements in molten steel [14,19–21]. As can be seen from the change of N content in Table 1, the increase in N content in molten steel from RH-end to tundish is below 4 ppm. During the whole producing process, the N contents in molten steel do not obviously increase and are all below 20 ppm. Consequently, the reoxidation caused by the absorbed air is basically excluded.

In addition, the inclusion amount and the T.O content in molten steel for Heat 1 do not increase when the same sponge titanium is added into steel. Hence, under this experimental condition, the ladle slag with high oxidability is the main reason for the serious reoxidation of molten steel. During the RH refining process, the molten steel driven by argon gas has better stirring conditions. Even when the slag is highly oxidizing, inclusions can float up more quickly. Therefore, the ND and AF of inclusions in two heats gradually decrease during RH treatment. At the holding stage, compared with the alloying time in RH, the holding time is usually more than 2 times as long, and the stirring strength of molten steel becomes weak. Because of the worse conditions for the floating up of inclusions and the

strong oxidized top slag, the molten steel may undergo serious reoxidation, leading to a significant increase in the ND and AF of inclusions in the tundish sample. For Heat 2, the T.Fe content in slag after RH reaches 18.1%, and the holding time is also more than 40 min. Before arriving at tundish, the oxygen in the ladle slag will transfer into the molten steel continuously, resulting in the deteriorated cleanliness of molten steel.

To sum up, in order to improve the cleanliness of molten steel, it is crucial to weaken the reoxidation by reducing the oxidability of slags and optimizing the steelmaking process during RH refining and tundish processes.

Figure 5 shows the size distribution of inclusions in Heat 1 and Heat 2 during RH treatment and tundish processes. From the figure, it can be seen that the ND of inclusions within 3 μm is the largest and the ND of inclusions above 5 μm has dropped to less than 2 mm^{-2}. Besides, the number of various inclusions appears to decrease with the increase in inclusion size. The number of Al_2O_3 and $Al_2O_3 \cdot TiO_x$ inclusions in Heat 1 keeps decreasing from the RH to tundish. However, in the tundish sample of Heat 2, the number of inclusions within 2 μm increases significantly owing to the serious reoxidation, which is also the main reason for the decrease in the mean size of Al_2O_3 inclusions. Meanwhile, it can be seen from the cumulative frequency distribution of inclusions that small-sized inclusions below 3 μm increase from around 77% before Ti addition to more than 81% after Ti addition. The long holding time between the removal of the ladle and the start of continuous casting gives inclusions the chance to grow and agglomerate. This results in a relatively strong increase in the percentage of the inclusions above 8 μm in tundish, which is a consequence of the maturation of the inclusion population. In other processes, the number of inclusions within 8 μm makes up almost 100%.

The Al_2O_3 cluster inclusions in IF steel are considered to be more harmful because of their larger size [22]. In the analyzing process of using ASPEX, many large-sized cluster-like inclusions may be defined as several inclusions, which will affect the accuracy of calculating the number of inclusions. In this study, a new method of determining the number of cluster inclusions is used to evaluate the cleanliness of IF steel. All Al_2O_3 and $Al_2O_3 \cdot TiO_x$ inclusions in the total detected area of a sample are assumed to be spherical, and then they are positioned on a map according to the location information of every inclusion. The relative size of the spherical dimension in the figure is determined depending on the size of inclusions, and multiple inclusions overlapping each other are considered as a cluster inclusion, and then the number of cluster inclusions can be counted.

The distribution of inclusions in the total sample detection area for Heat 1 and Heat 2 during RH treatment and tundish processes is shown in Figure 6. In the sample of RH-1, there are many small-sized inclusions aggregated together to form a cluster, including 38 clusters in Heat 1 and 21 clusters in Heat 2. During the period after Ti addition, the number of cluster inclusions decreases significantly because some larger inclusions have floated up and been removed. The single inclusion of forming the cluster is also larger in size, and even some inclusions are over 10 μm. After finishing the holding stage, compared with Heat 1, the number of cluster inclusions in the tundish sample of Heat 2 reaches 19, indicating that there are many cluster inclusions existing in the molten steel when the molten steel undergoes serious reoxidation. In the meantime, for Heat 1, the number of single inclusions in the tundish sample decreases obviously from Figure 6. However, the number of single inclusions below 4 μm in the tundish sample of Heat 2 has a significant increase, so the size of inclusions decreases significantly, as described in Figure 2. Additionally, the number of clusters obtained by this method is in good agreement with the ND and AF of inclusions in Figures 2 and 3, indicating that it is relatively reasonable.

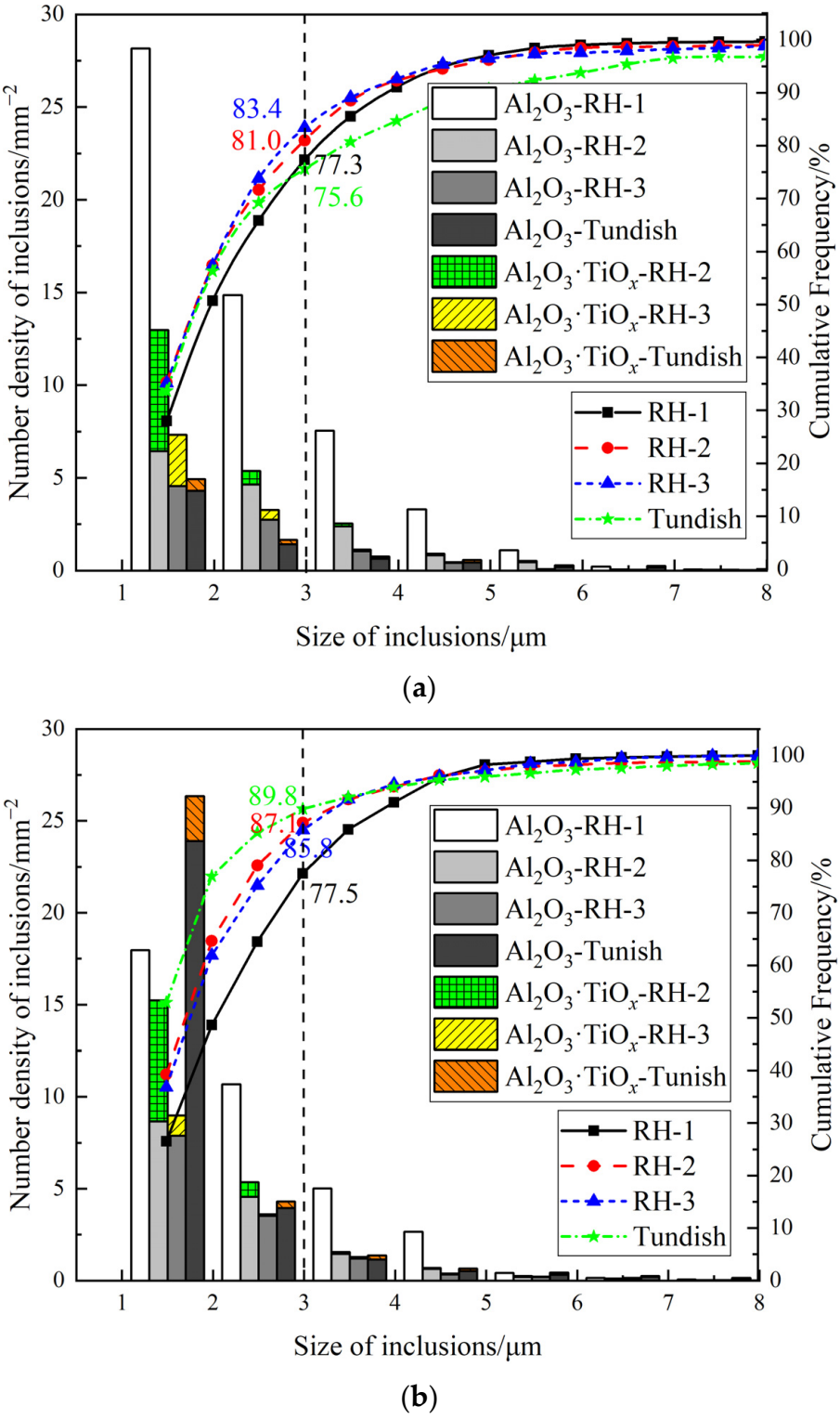

Figure 5. Size distribution of inclusions in (**a**) Heat 1 and (**b**) Heat 2 during RH treatment and tundish processes.

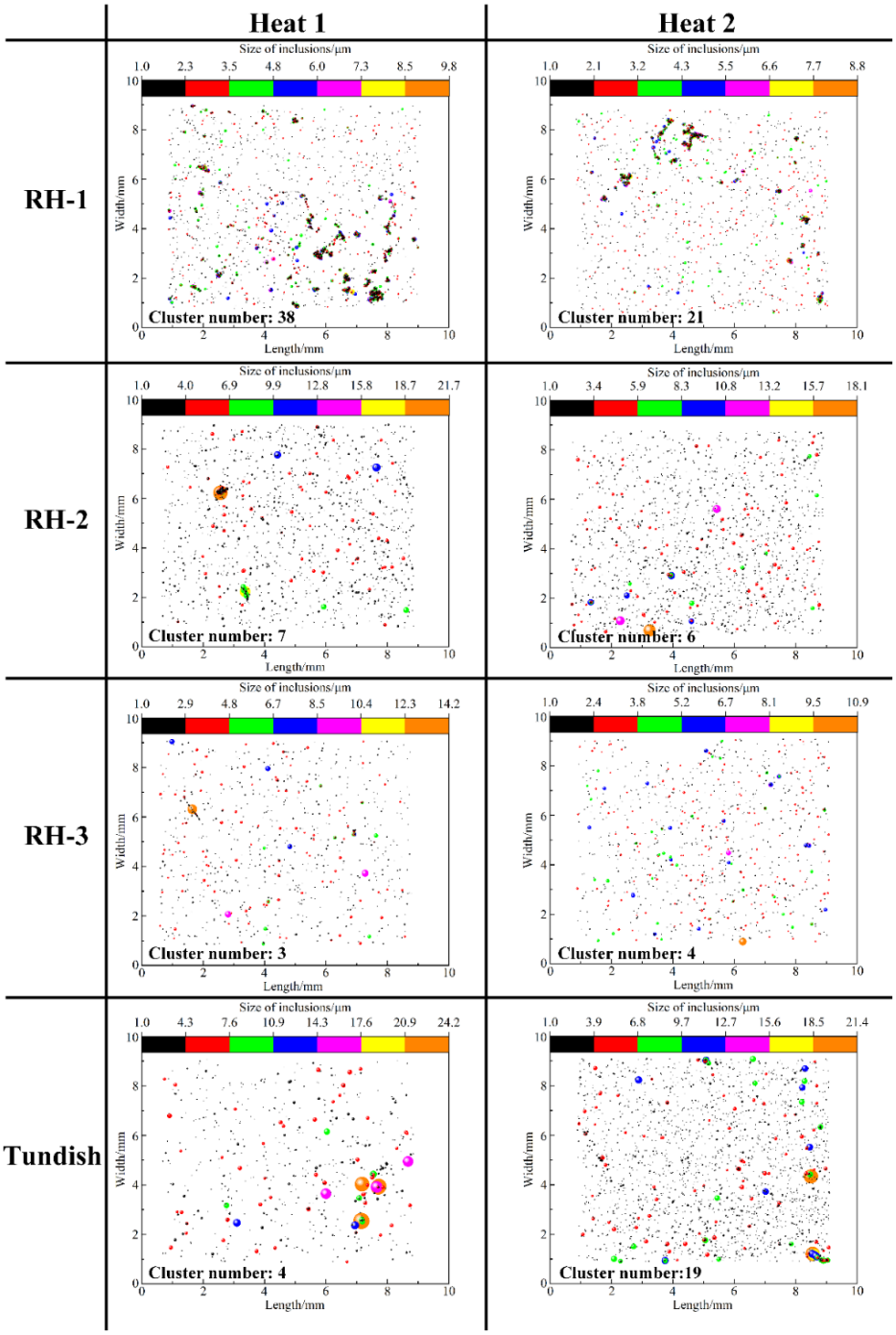

Figure 6. Distribution of inclusions in the total sample detection area for Heat 1 and Heat 2 during RH treatment and tundish processes.

3.2. Morphological Evolution of Inclusions

The morphological evolution of Al_2O_3 inclusions in molten steel from RH to tundish is depicted in Figure 7. Once the Al is added into the molten steel during the RH process, a large number of small-sized Al_2O_3 inclusions with different shapes are formed in molten steel, including spherical, bar-like, polygonal and other irregular shapes. These inclusions begin to aggregate together to form large Al_2O_3 clusters as shown in Figure 7 (RH-1). At around 3 min after Al addition, these small-sized Al_2O_3 inclusions cannot float up rapidly, and the ND of Al_2O_3 inclusions reaches more than 35 mm^{-2}. This indicates that it will take a longer time to further polymerize and grow to be removed for these inclusions.

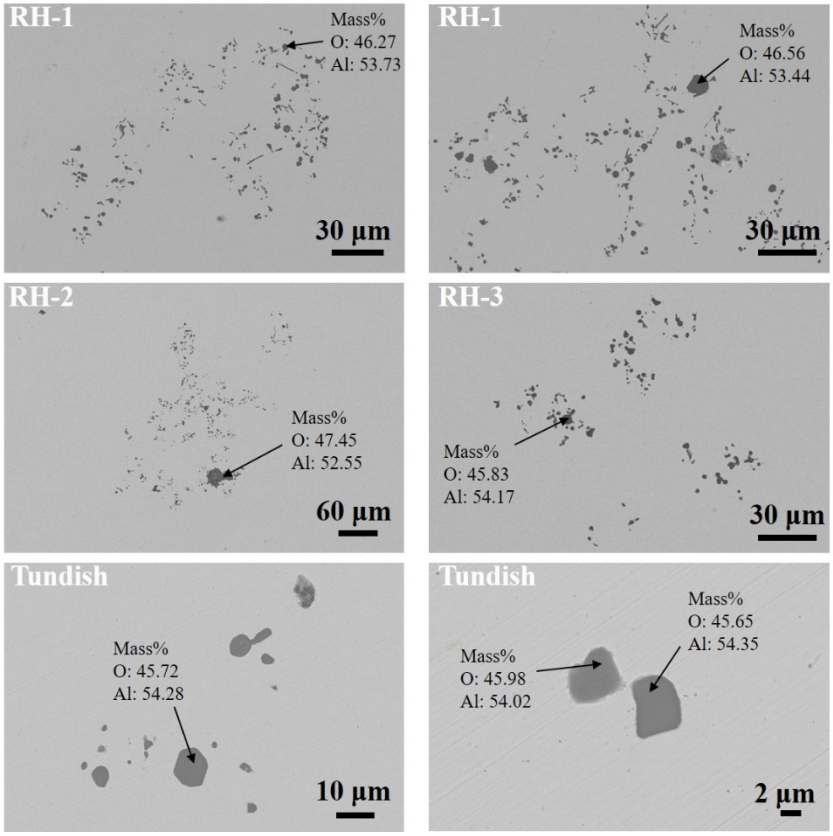

(**a**)

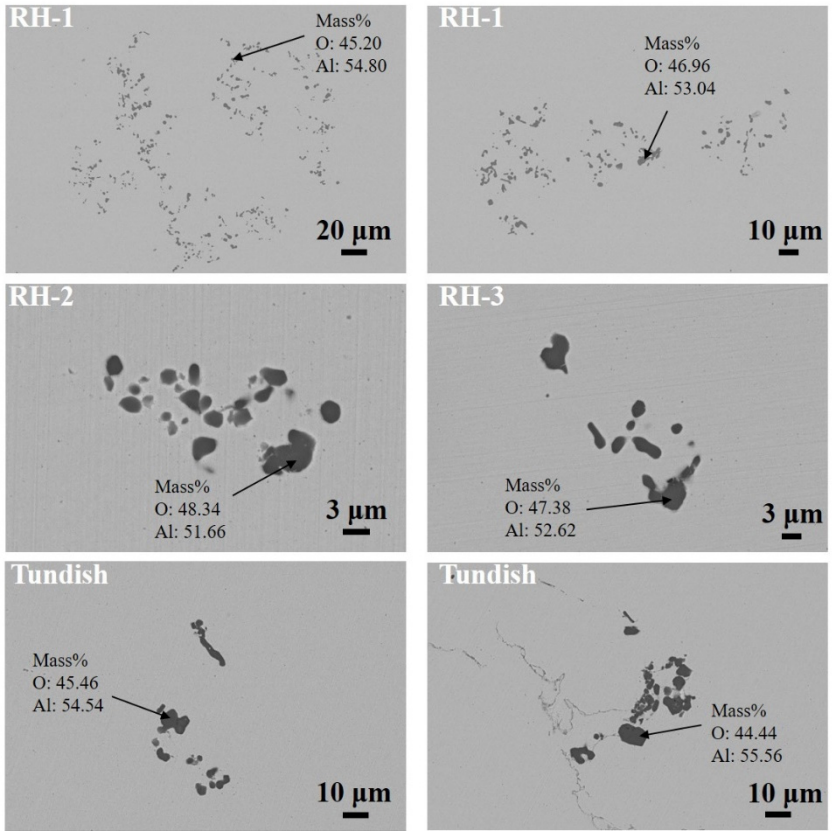

(**b**)

Figure 7. Morphologies of Al_2O_3 inclusions during RH treatment and tundish processes. (**a**) Heat 1, (**b**) Heat 2.

After Ti addition, there is still a certain amount of Al_2O_3 clusters in molten steel, as shown in Figure 7 (RH-2 and RH-3). Few Al_2O_3 inclusions can react with Ti in molten steel to form $Al_2O_3{\cdot}TiO_x$ inclusions, and most of the clusters are still pure Al_2O_3 inclusions. The size of the Al_2O_3 cluster decreases significantly at the end of RH, and the ND of Al_2O_3 inclusions in molten steel drops to less than 15 mm^{-2}, which is a combined result of the larger inclusions being removed more rapidly from molten steel through floatation and smaller inclusions precipitating. The decreasing trend of the T.O content in molten steel is consistent with the above evolution characteristic of inclusions, and it can be speculated that the Al deoxidation process at about 6 min after Ti addition could be completed because the oxygen level is close to the equilibration at the end of RH.

In the tundish sample, few cluster-like Al_2O_3 inclusions in molten steel of Heat 1 are found, and the Al_2O_3 inclusions mostly exist as single particles. Meanwhile, many Al_2O_3 clusters still exist in molten steel of Heat 2, as shown in Figure 7 (tundish). According to the analysis results in Section 3.1, this is mainly due to the serious reoxidation of molten steel caused by the ladle slag with high oxidation and the long holding time.

Figure 8 shows morphologies of $Al_2O_3{\cdot}TiO_x$ inclusions during RH treatment and tundish processes, indicating that there are mainly three types of $Al_2O_3{\cdot}TiO_x$ inclusions. The first type is similar to the shape of Al_2O_3 inclusions, including spherical and polygonal shapes, and the size is usually smaller than 5 μm, as shown in Figure 8a–d. The other two types of $Al_2O_3{\cdot}TiO_x$ inclusions are substantially spherical and relatively large in size, as shown in Figure 8e–l. Figure 9 shows the elemental mapping of $Al_2O_3{\cdot}TiO_x$ inclusions during RH treatment and tundish processes. In the first type, an Al-Ti-O corner is distributed on the surface of the Al_2O_3 inclusion, and the morphology and composition are nearly identical to pure alumina inclusions, as shown in Figure 9a,b. In the second type, inclusions with traces of Al and Ti are homogeneously distributed, as shown in Figure 9c–e, and some inclusions such as those in Figure 9c,e are surrounded by an Al_2O_3 layer with an Al-Ti-O core. In the third type, there are heterogeneous Al-Ti-O inclusions with an irregular Al_2O_3 core and an Al-Ti-O or TiO_x surrounding layer, as shown in Figure 9f,g, and the size is the largest of the three types.

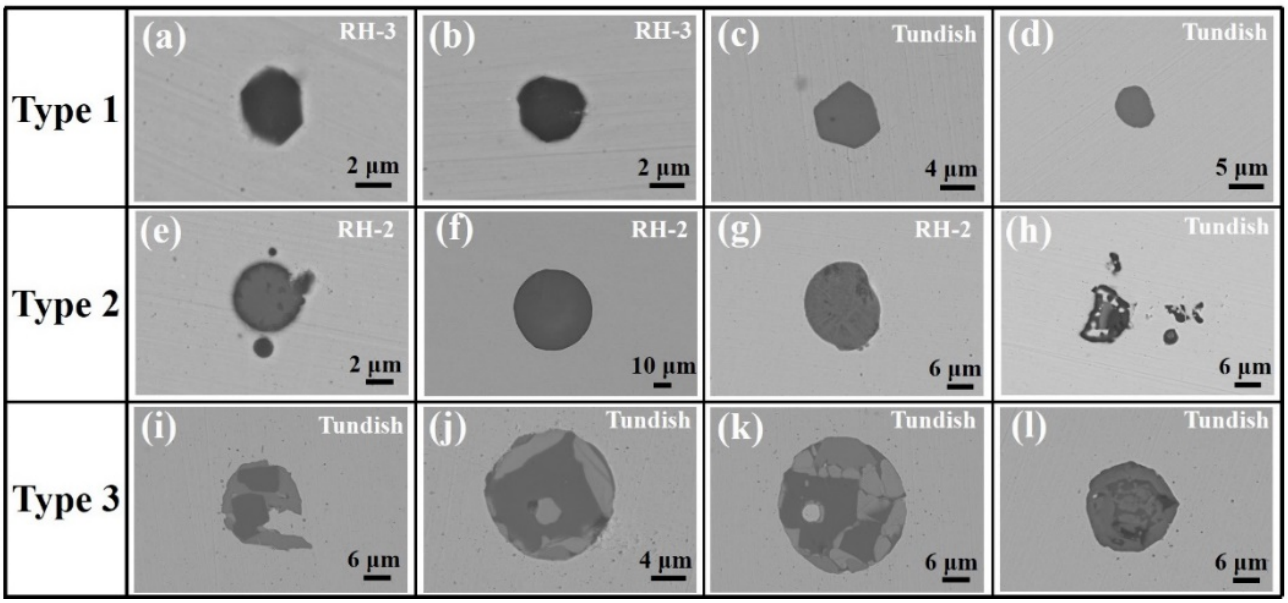

Figure 8. Morphologies of $Al_2O_3{\cdot}TiO_x$ inclusions during RH treatment and tundish processes. (**a**–**d**) Type 1 of $Al_2O_3{\cdot}TiO_x$ inclusions, (**e**–**h**) Type 2 of $Al_2O_3{\cdot}TiO_x$ inclusions, (**i**–**l**) Type 3 of $Al_2O_3{\cdot}TiO_x$ inclusions.

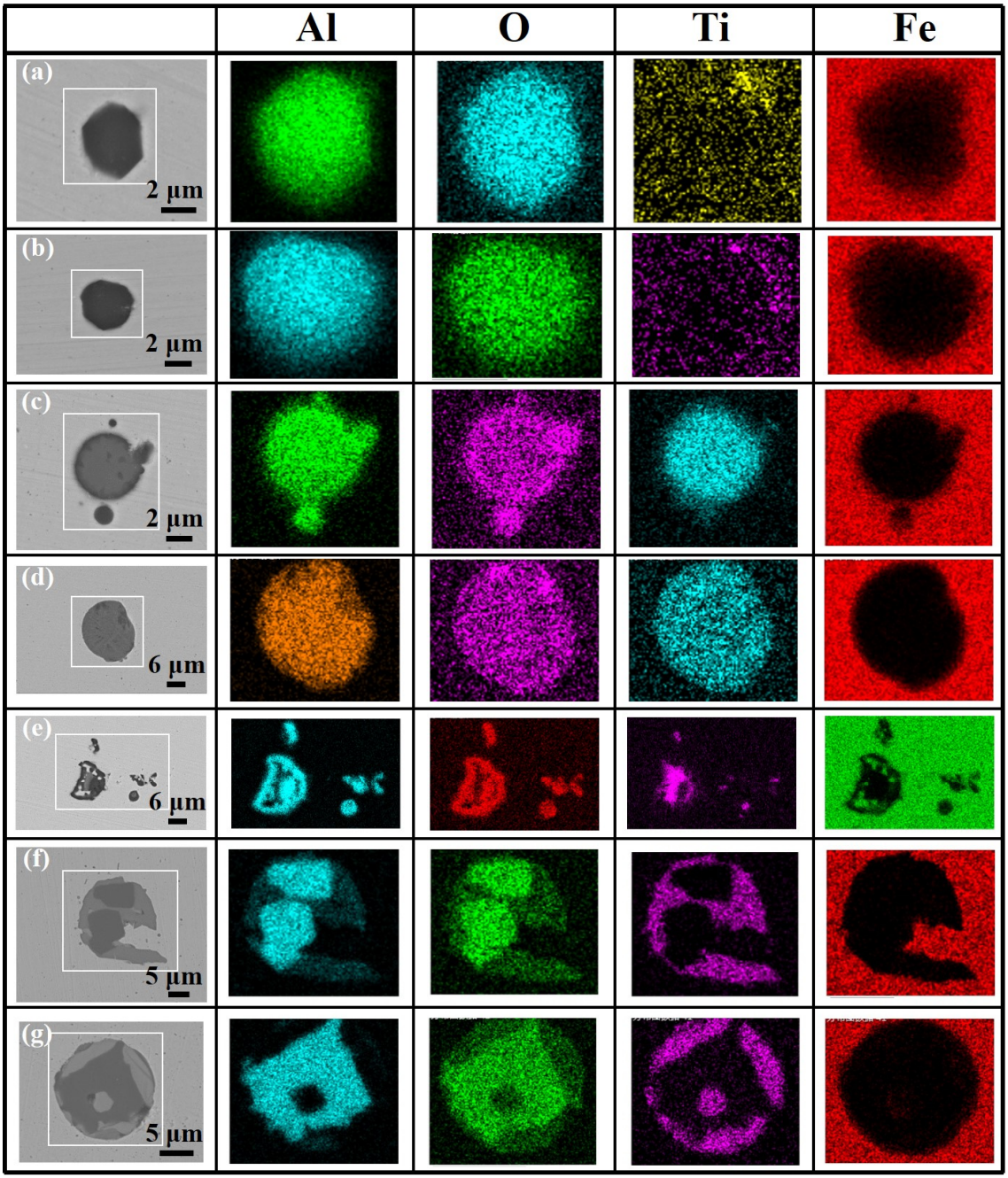

Figure 9. Elemental mapping of $Al_2O_3 \cdot TiO_x$ inclusions during RH treatment and tundish processes. (**a**,**b**) elemental mapping of Type 1 inclusions, (**c**–**e**) elemental mapping of Type 2 inclusions, (**f**,**g**) elemental mapping of Type 3 inclusions.

Similar morphologies of the first two types of $Al_2O_3 \cdot TiO_x$ inclusions were observed by Dorrer [19], Yang [23], Wang [24], Bai [25] and Yang [26]. The third type of $Al_2O_3 \cdot TiO_x$ inclusions, in which the Al-Ti-O is distributed in the outer part and the Al_2O_3 is distributed in the inner part, was also reported by Basu [14], Park [20], Wang [27], Doo [28], Qin [29] and Sun [30]. Furthermore, it is worth discussing the formation mechanism of different types of inclusions later.

The percentage of various $Al_2O_3 \cdot TiO_x$ inclusions during RH treatment and tundish processes is shown in Figure 10. From the figure, it can be seen that there are mainly two types of titanium-containing inclusions, namely Type 1 and Type 2, after Ti addition during the RH refining process. At 3 min after Ti addition, Type 1 of $Al_2O_3 \cdot TiO_x$ inclusions in two

heats accounts for 83.8% and 93.2%, respectively. At the end of RH refining, the percentage of Type 1 inclusions decreases, and the percentage of Type 2 inclusions begins to increase. In the two tundish samples, Type 3 of $Al_2O_3 \cdot TiO_x$ inclusions appears, but the number of Type 3 inclusions is significantly lower than that of the other two types. Meanwhile, the proportion of Type 1 inclusions further decreases, and the proportion of Type 2 inclusions further increases. This is mainly because under the good-stirring conditions in molten steel after Ti addition, the process of Ti reducing Al to form $Al_2O_3 \cdot TiO_x$ inclusions has been proceeding, and thus more and more $Al_2O_3 \cdot TiO_x$ inclusions with relatively uniform composition are generated. In addition, for the tundish samples, the total amount of inclusions in Heat 2 is larger, and the number of Type 1 and Type 2 inclusions in Heat 2 is significantly more than that in Heat 1, which is caused by the serious reoxidation process of molten steel. Therefore, the types of $Al_2O_3 \cdot TiO_x$ inclusions generated in molten steel are not only related to the existence of Ti in molten steel, but also closely related to the reoxidation process of molten steel caused by the excessively high oxidability of top slag.

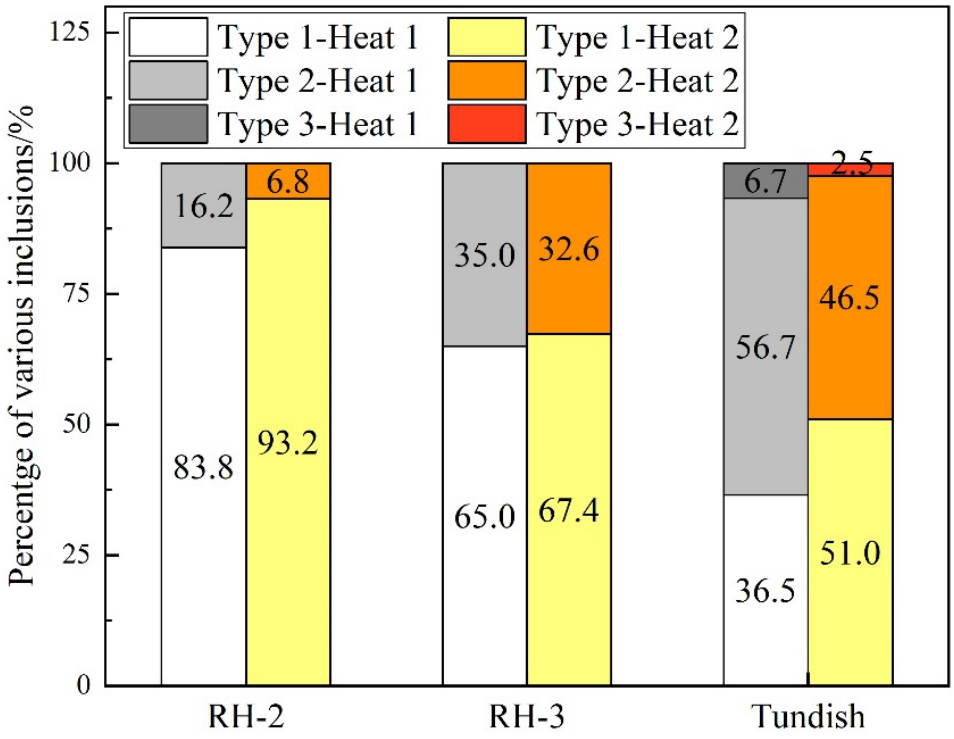

Figure 10. Percentage of various $Al_2O_3 \cdot TiO_x$ inclusions during RH treatment and tundish processes.

The Ti/Al ratio in various $Al_2O_3 \cdot TiO_x$ inclusions during RH treatment and tundish processes is presented in Figure 11. During the whole steelmaking process, the Ti content in Type 2 and Type 3 inclusions is significantly larger than that in Type 1 inclusions, and the Ti and Al contents in Type 1 inclusions almost keep constant. During RH treatment, the Ti and Al contents in Type 2 inclusions have a small fluctuation. After arriving at tundish, the Ti/Al ratio in Type 2 inclusions increases significantly owing to the increase in Ti content. In the tundish sample, the Ti/Al ratio of Type 3 inclusions among the three types of $Al_2O_3 \cdot TiO_x$ inclusions reaches the maximum, indicating that the relative Ti content in Type 3 inclusions is at the largest level. Additionally, the Ti/Al ratio of Type 2 and Type 3 inclusions in the tundish sample of Heat 2 is larger than that in the tundish sample of Heat 1. This indicates that the Ti content in Type 2 and Type 3 inclusions will increase obviously when the molten steel encounters serious reoxidation.

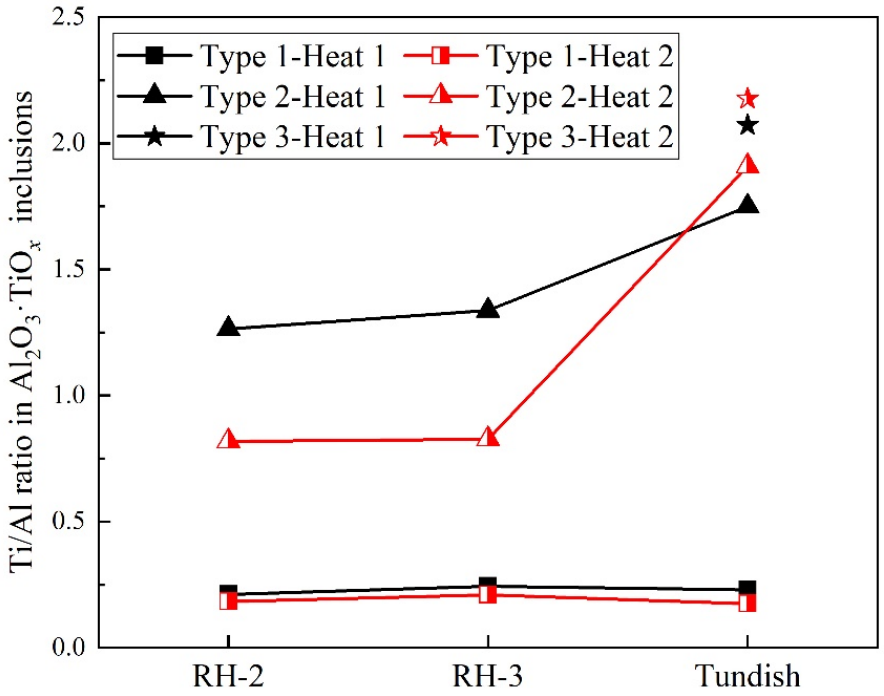

Figure 11. Ti/Al ratio in various Al_2O_3·TiO_x inclusions during RH treatment and tundish processes.

3.3. Formation Evolution of Inclusions

Most research studies in this field have focused on the formation evolution of Al_2O_3 inclusions created in the laboratory through small furnace trials [31–33]. However, the formation of Al_2O_3 clusters in the industrial steelmaking process should be studied more completely. It is well known that nucleation, growth and removal of inclusions during the deoxidation process determine the size distribution of the inclusion population. The formation and removal mechanisms of Al_2O_3 inclusions during RH refining and tundish processes are depicted in Figure 12. Al_2O_3 inclusions below 1 μm can nucleate quickly after starting deoxidation. At around 3 min after Al addition, these tiny Al_2O_3 particles in molten steel grow, collide with each other and aggregate to form the large Al_2O_3 cluster as shown in Figure 7 (RH-1).

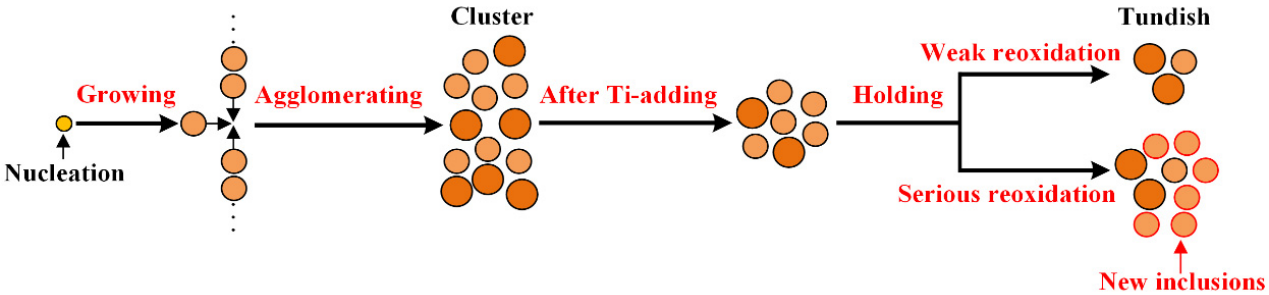

Figure 12. Formation and removal mechanisms of Al_2O_3 inclusions during RH refining and tundish processes.

During the pure circulation period after Ti addition, many large-sized Al_2O_3 inclusions have been removed, and some small-sized Al_2O_3 clusters still exist in molten steel, as shown in Figure 7 (RH-2 and RH-3). When the slag oxidability is relatively low with the weak reoxidation process during the holding process, the cleanliness of molten steel will not deteriorate, and most of the Al_2O_3 inclusions form single inclusion particles, as shown in the tundish sample of Figure 7a. Nevertheless, when the unstable oxide contents (FeO, MnO, SiO_2) in the ladle slag are large and the holding time is also relatively long, the molten

steel will undergo serious reoxidation and the cleanliness of molten steel will deteriorate. There are many small-sized Al_2O_3 inclusions formed by the reoxidation process, so it can be seen in Figure 7b that there are still some Al_2O_3 clusters in the tundish sample.

The mechanism of the reoxidation process of molten steel by the top slag during the holding stage is shown in Figure 13. When the unstable oxide contents (FeO, MnO, SiO_2) in the top slag are at a high level, the oxygen can transfer continuously into molten steel at the steel/slag interface. Thus, the [Al] in molten steel combines with the oxygen at the steel/slag interface to form Al_2O_3 inclusions, according to Reaction (R1). In the meantime, the [Al] and [Ti] in molten steel may also react with the oxygen at the steel/slag interface, resulting in the formation of $Al_2O_3{\cdot}TiO_x$ inclusions, based on Reaction (R2). The morphologies of $Al_2O_3{\cdot}TiO_x$ inclusions formed by the reoxidation process are mainly the Type 1 and Type 2 inclusions as shown in Figure 8. The number of Type 3 $Al_2O_3{\cdot}TiO_x$ inclusions is relatively low as described in Figure 10, and the formation conditions are fairly limited during the reoxidation process, which will be explained in detail below. In addition, the formation of TiO_x inclusions is possible at the steel/slag interface based on Reaction (R3).

$$2[\mathrm{Al}] + 3[\mathrm{O}]^* = \mathrm{Al_2O_3} \quad \text{(R1)}$$

$$2[\mathrm{Al}] + [\mathrm{Ti}] + (x+3)[\mathrm{O}]^* = \mathrm{Al_2O_3 \cdot TiO_x} \quad \text{(R2)}$$

$$[\mathrm{Ti}] + x[\mathrm{O}]^* = \mathrm{TiO_x} \quad \text{(R3)}$$

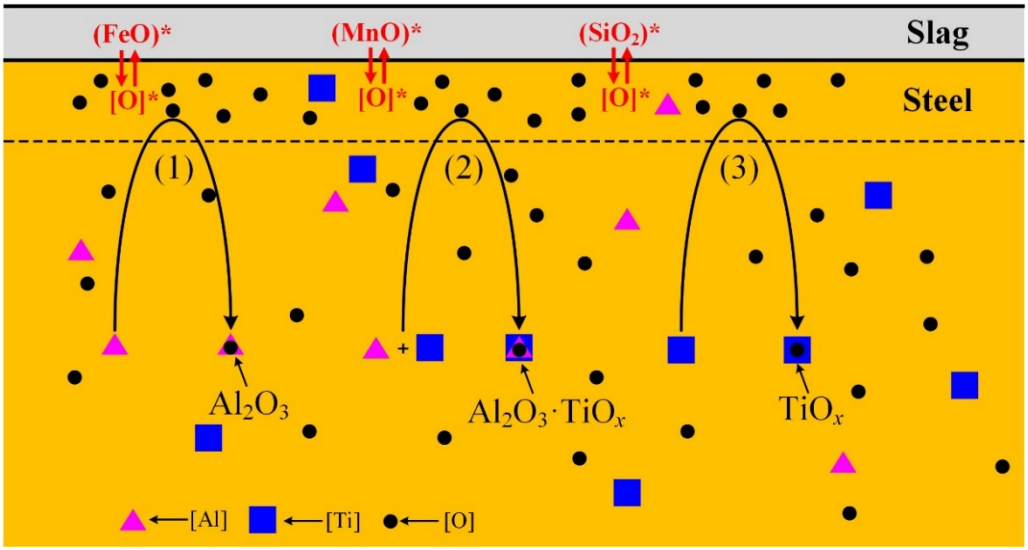

Figure 13. Mechanism of the reoxidation process of molten steel by the top slag during the holding stage.

Many scholars [23–30] have studied the formation mechanism of $Al_2O_3{\cdot}TiO_x$ inclusions, and their studies are good for analyzing the formation mechanisms of various $Al_2O_3{\cdot}TiO_x$ inclusions. The schematic of the process is depicted in Figure 14. The $Al_2O_3{\cdot}TiO_x$ inclusions formed by mechanisms I and II usually exist in the melt away from the steel/steel interface. After Ti feeding into molten steel, the formation of a local high [Ti] region provides the possibility of generation of Al-Ti-O or TiO_x inclusions based on Reactions (R4) and (R5). The reaction area between the high [Ti] region and the inclusion surface determines the final morphology of $Al_2O_3{\cdot}TiO_x$ inclusions. When only part of the area around Al_2O_3 inclusions is a high [Ti] region, the Al_2O_3 inclusion is only partially reduced by [Ti] with time, thus forming the Type 1 inclusions in Figure 8a–d, and the formation mechanism is depicted in Figure 14I.

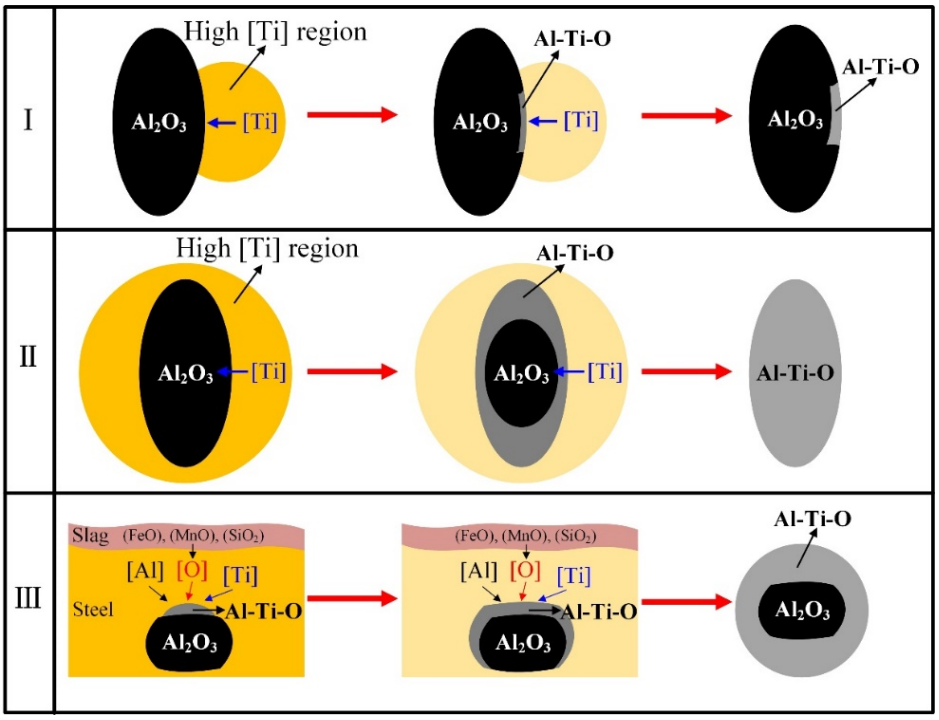

Figure 14. Formation mechanisms of $Al_2O_3{\cdot}TiO_x$ inclusions during RH refining and tundish processes. (**I**) first formation mechanism of $Al_2O_3{\cdot}TiO_x$ inclusions, (**II**) second formation mechanism of $Al_2O_3{\cdot}TiO_x$ inclusions, (**III**) third formation mechanism of $Al_2O_3{\cdot}TiO_x$ inclusions.

When the Al_2O_3 inclusion is completely covered by the high [Ti] region, the Al_2O_3 inclusion will gradually be reduced from the outside to the inside, thus forming the Type 2 inclusions as shown in Figure 8e–h. The formation mechanism of the inclusions is depicted in Figure 14II. After that, with the progress of reduction of Al_2O_3, a low [Ti] region around the inclusion exists. Thus, the $Al_2O_3{\cdot}TiO_x$ inclusion may transfer to Al_2O_3 from the surface to the inner part of the inclusion according to Reactions (R4) and (R5). As a result, the inclusion with an Al-Ti-O core surrounded by a Al_2O_3 layer forms finally, as shown in Figure 8e,h.

$$xAl_2O_3 + 3[Ti] = 3TiO_x + 2x[Al] \quad (R4)$$

$$5Al_2O_3 + 3[Ti] = 3Al_2TiO_5 + 4[Al] \quad (R5)$$

$$4[Al] + 3Al_2TiO_5 = 3[Ti] + 5Al_2O_3 \quad (R6)$$

$$2x[Al] + 3TiO_x = 3[Ti] + xAl_2O_3 \quad (R7)$$

The third type of $Al_2O_3{\cdot}TiO_x$ inclusions mainly exists in the tundish process. Previous studies [14,20,28,30] have pointed out that these inclusions are closely related to the reoxidation of molten steel, and the top slag with strong oxidability in this steel plant during the smelting process also provides conditions for the formation of such inclusions. The formation mechanism of the inclusions is depicted in Figure 14III. The ladle or tundish slag with high unstable oxide contents keeps transferring oxygen into molten steel, and the oxygen reacts with [Al] and [Ti] in molten steel to form the Al-Ti-O inclusion on the surface of the irregular Al_2O_3 inclusions according to Reaction (R2). Finally, the spherical inclusions partially or completely wrapped by the Al-Ti-O inclusion on the surface of pure Al_2O_3 inclusions appear in molten steel. Because of the continuous reoxidation process, newly formed Al-Ti-O inclusions accumulate constantly on the surface, so the size is also larger than the previous two types.

Interestingly, these irregular Al_2O_3 inclusions in Type 3 inclusions are usually larger in size as shown in Figure 8i–l, and they are unlikely to be generated from the reoxidation process. It is more likely that the Al_2O_3 inclusions accumulate and grow in the melt,

then float up to the steel/slag interface and finally become the nucleation core of Type 3 inclusions. However, the number of Type 3 inclusions is relatively small, indicating that most of the mature Al_2O_3 inclusions have been absorbed by the top slag. According to the above analysis results, the number of Al_2O_3 inclusions formed by the reoxidation is significantly larger than that of $Al_2O_3{\cdot}TiO_x$ inclusions formed by the reoxidation. Combining Figure 13 with Figure 14, the $Al_2O_3{\cdot}TiO_x$ inclusions can not only form directly at the steel/slag interface, but also there is an indirect way of forming $Al_2O_3{\cdot}TiO_x$ inclusions in the case of serious reoxidation of molten steel. Specifically, the Al_2O_3 inclusions formed by the reoxidation form at the steel/slag interface firstly, and then these new Al_2O_3 particles scatter in the melt. Eventually, these Al_2O_3 particles may be transferred into $Al_2O_3{\cdot}TiO_x$ inclusions under the action of the high [Ti] region.

The equilibrium phase diagram for the Fe-Al-Ti-O system at 1873 K was calculated by using Factsage 7.2 with the FactPS, FToxid and FSstel databases in September 2020, as depicted in Figure 15. The black dot in Figure 15 represents the IF steel composition in the current work, indicating that Al_2O_3 is the only thermodynamically stable phase under the experimental conditions. From the figure, it can be seen that different types of Al-Ti-O inclusions have various modification mechanisms. The Type 1 and Type 2 of Al-Ti-O inclusions can be formed by the increase in the local [Ti] concentration, and the red solid arrow can represent the formation mechanisms of I and II in Figure 14. Meanwhile, the reoxidation of molten steel by the ladle or tundish slag leads to an increase in the dissolved oxygen and total oxygen in molten steel, and thus it is possible to generate directly or indirectly three types of Al-Ti-O inclusions, as presented by the blue solid arrow in Figure 15. In addition, with the uniformity of the molten steel composition, the Al-Ti-O inclusion may eventually be partially or fully turned into the Al_2O_3 inclusion by Al reducing, as shown by the green dashed arrow in Figure 15.

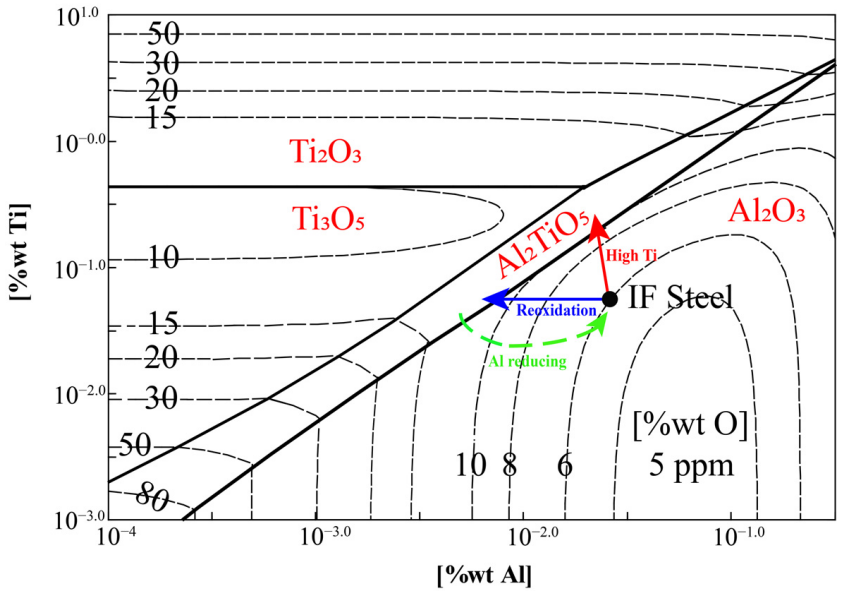

Figure 15. The equilibrium phase diagram for the Fe-Al-Ti-O system at 1873 K.

3.4. Influence of Process Parameters on the Cleanliness of Molten Steel

The secondary refining process is considered to be the main place for the removal of inclusions in molten steel, and the percentage of inclusions removed accounts for more than 70% [34]. Recently, to improve the cleanliness of molten steel, reducing the number of endogenous inclusions, improving the removal efficiency of inclusions and lessening the external inclusions caused by the reoxidation are dominant ways during the RH refining process. For this reason, studying the influence of relevant process parameters on the removal efficiency of inclusions is vital to improve the quality of the products.

The [O] content in molten steel before Al deoxidation is a key parameter that determines the amount of Al added and the number of inclusions in molten steel [15,34]. Figure 16 shows the relationship between the number of inclusions after RH and [O] content in molten steel before Al deoxidation. As shown in the figure, with the increase in the [O] content in molten steel, the number of inclusions in molten steel after RH tends to increase, and the cleanliness of molten steel becomes worse.

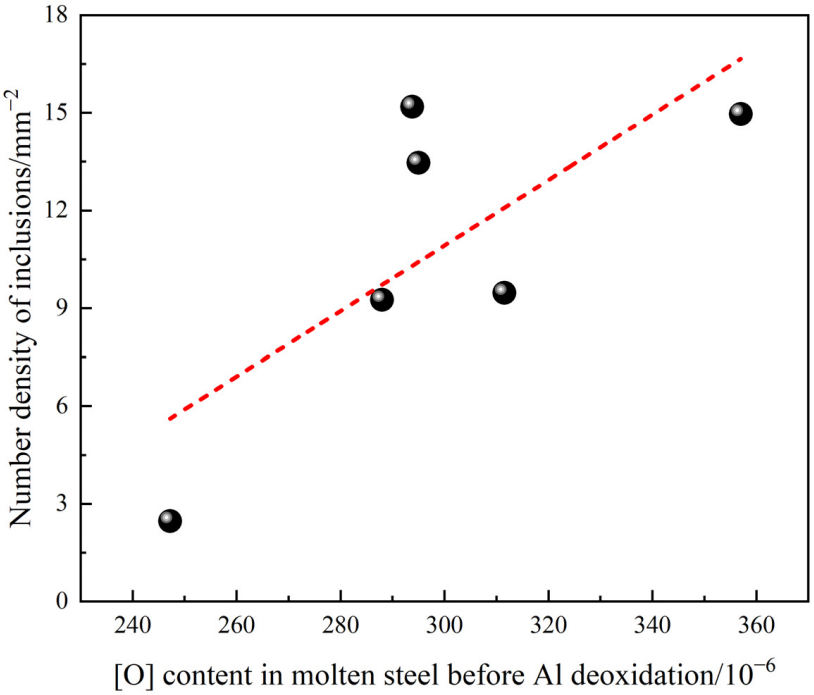

Figure 16. Relationship between the number of inclusions after RH and [O] content in molten steel before Al deoxidation.

According to the research of Wakoh [35], all dissolved oxygen was consumed for forming spherical inclusions, and the relationship between the oxygen content in molten steel and the number of inclusions in molten steel was obtained, as shown in Equation (3).

$$\frac{4}{3}\pi r^3 \rho_i N_i \left(\frac{3M_O}{M_i}\right) = \left(\frac{C_O}{10^6}\right) W_{Fe} \quad (3)$$

where r is the radius of inclusion, m; ρ_i is the density of inclusion, kg·m^{-3}; the density of Al_2O_3 inclusions is taken as 3.97 × 10^3 kg·m^{-3} [27]; M_O is the molar weight of oxygen, g·mol^{-1}; M_i is the molar weight of inclusion, g·mol^{-1}; C_O is the concentration of oxygen, 10^{-6}; and W_{Fe} is the total weight of molten steel, kg.

The relationship between the number of Al_2O_3 inclusions and [O] content in molten steel before Al deoxidation is depicted in Figure 17. From the figure, it can be seen that the number of Al_2O_3 particles formed in molten steel increases gradually with the gradual increase in dissolved oxygen in molten steel before Al deoxidation, and the increased amplitude is more obvious with the decreased radius of Al_2O_3 inclusions. In this paper, the average diameter of Al_2O_3 inclusions in these samples at 3 min after Al addition is only about 2 μm. Therefore, reducing the dissolved oxygen content before Al deoxidation has a significant effect on reducing the number of Al_2O_3 inclusions. Combining Figure 16 with Figure 17, it can be seen that reducing the dissolved oxygen content before Al deoxidation is beneficial to improve the cleanliness of molten steel.

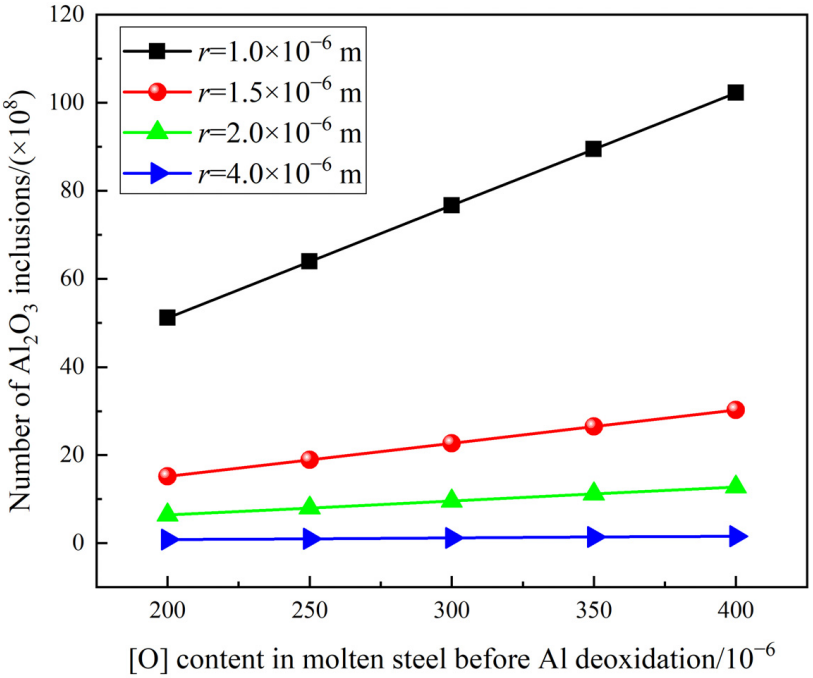

Figure 17. Relationship between the number of Al_2O_3 inclusions and [O] content in molten steel before Al deoxidation.

Figure 18 shows changes in the ND of inclusions, T.Fe content after RH and holding time in different heats. When the T.Fe content is above 15% and the holding time is more than 30 min, the ND of inclusions in molten steel is more than 9 mm^{-2}. However, when the holding time is less than 30 min or the T.Fe content of slag is below 15%, the number of inclusions in molten steel is relatively low. Therefore, it is beneficial to weaken the reoxidation process of molten steel and improve the cleanliness of molten steel by minimizing the holding time and reducing the oxidability of slag after RH.

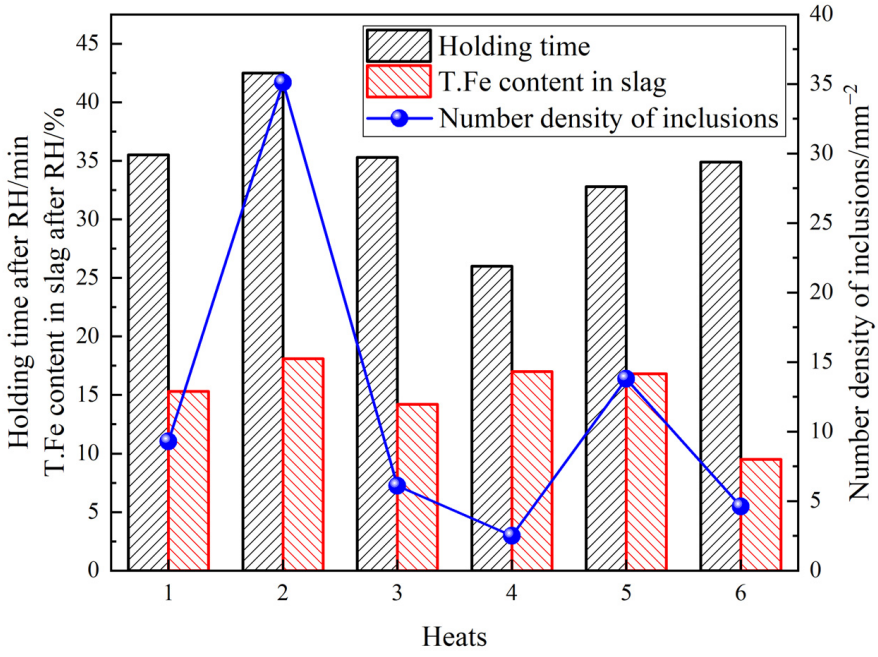

Figure 18. Changes in number density of inclusions, T.Fe content after RH and holding time in different heats.

4. Conclusions

Considering Ti-bearing IF steel produced via the BOF–LF–RH–CC process, the evolution of inclusions in molten steel during RH refining to tundish was analyzed through a systematic sampling experiment, and the influence of reoxidation process and process parameters on the cleanliness of molten steel was also studied. The results are summarized as follows:

(1) During RH treatment, the ND and AF of Al_2O_3 and $Al_2O_3 \cdot TiO_x$ inclusions decrease gradually. In the tundish samples, when the ND and AF of Al_2O_3 and $Al_2O_3 \cdot TiO_x$ inclusions especially from 1 to 2 μm increase significantly, the mean size of all inclusions shows a decreasing trend.

(2) The deteriorated cleanliness of molten steel is closely related to the serious reoxidation of molten steel caused by the slag with high oxidability during the holding process. Meanwhile, the number of clusters counted by the location maps shows basically the same trend with the ND and AF of inclusions.

(3) During the whole steelmaking process, Type 1 and Type 2 inclusions are the main two types of titanium-containing inclusions. In the tundish sample with serious reoxidation, there are still some small-sized Al_2O_3 clusters, and the number of Type 1 and Type 2 inclusions and Ti content of Type 2 and Type 3 inclusions will increase obviously.

(4) In the case of serious reoxidation, $Al_2O_3 \cdot TiO_x$ inclusions can not only form directly at the steel/slag interface, but also form indirectly: Al_2O_3 particles generated from reoxidation may be transferred into $Al_2O_3 \cdot TiO_x$ inclusions under the action of a local high [Ti] region.

(5) It is beneficial to weaken the reoxidation process and improve the cleanliness of molten steel by reducing the oxygen content in molten steel before Al deoxidation, minimizing the holding time and reducing the slag oxidability after RH.

Author Contributions: Conceptualization, B.Y. and J.L.; Methodology, B.Y. and J.L.; Software, B.Y.; Validation, B.Y., J.L. and J.Z.; Formal Analysis, B.Y.; Investigation, B.Y. and M.Z.; Resources, B.Y., J.L. and J.Z.; Data Curation, B.Y., J.H. and X.Y.; Writing—Original Draft Preparation, B.Y.; Writing—and Editing, B.Y.; Visualization, B.Y.; Supervision, J.L., J.Z. and M.Z.; Project Administration, J.L., J.Z., J.H. and X.Y.; Funding Acquisition, J.L., J.Z. and J.H. All authors have read and agreed to the published version of the manuscript.

Funding: The research was funded by the National Natural Science Foundation of China, grant number 51874028.

Data Availability Statement: Not applicable.

Acknowledgments: The authors would like to thank Pangang Group Xichang Steel and Vanadium Corporation Limited for providing technical and financial support. The authors gratefully acknowledge Pangang Group Research Institute Corporation Limited for the help and support with the ASPEX analysis.

Conflicts of Interest: The authors declare no conflict of interest. The funding sponsors had no role in the choice of the research project; the design of the study; the collection, analysis or interpretation of data; the writing of the manuscript; or the decision to publish the results.

References

1. Wang, C.; Nuhfer, N.T.; Sridhar, S. Transient behavior of inclusion chemistry, shape, and structure in Fe-Al-Ti-O melts: Effect of titanium source and laboratory deoxidation simulation. *Metall. Mater. Trans. B* **2009**, *40*, 1005–1021. [CrossRef]
2. Wang, C.; Nuhfer, N.T.; Sridhar, S. Transient behavior of inclusion chemistry, shape, and structure in Fe-Al-Ti-O melts: Effect of titanium/aluminum ration. *Metall. Mater. Trans. B* **2009**, *40*, 1022–1034. [CrossRef]
3. Deng, X.X.; Ji, C.X.; Zhu, G.S.; Liu, Q.M.; Huang, F.X.; Tian, Z.H.; Wang, X.H. Quantitative evaluations of surface cleanliness in IF Steel slabs at unsteady casting. *Metall. Mater. Trans. B* **2019**, *50*, 1974–1987. [CrossRef]
4. Matsuura, H.; Wang, C.; Wen, G.H.; Sridhar, S. The transient stages of inclusion evolution during Al and/or Ti additions to molten iron. *ISIJ Int.* **2007**, *47*, 1265–1274. [CrossRef]

5. Deng, X.X.; Liu, G.L.; Wang, Q.Q.; Liu, B.S.; Ji, C.X.; Li, H.B.; Shao, X.J.; Zhu, G.S. Effect of the weir structure in the tundish on the cleanliness of IF steels and elimination of spot-like defects in deep drawing automobile steel sheets. *Metall. Res. Technol.* **2020**, *117*, 609. [CrossRef]
6. Deng, X.X.; Ji, C.X.; Guan, S.K.; Wang, L.C.; Xu, J.F.; Tian, Z.H.; Cui, Y. Inclusion behaviour in aluminium-killed steel during continuous casting. *Ironmak. Steelmak.* **2019**, *46*, 1428420. [CrossRef]
7. Choucair, H.; Zhou, J.Z.; Ali Jawad, B.; Liu, L.P. Study of the fatigue failure of engine valve springs due to non-metallic inclusions. *SAE Int.* **2012**, *5*, 388–394. [CrossRef]
8. Murakami, Y. *Metal Fatigue: Effects of Small Defects and Nonmetallic Inclusions*, 2nd ed.; Elsevier: London, UK, 2002; pp. 681–682.
9. Story, S.R.; Goldsmith, G.E.; Klepzig, G.L. Study of cleanliness and castability in Ti-stabilized ultra low carbon steels using automated SEM inclusion analysis. *Metall. Res. Technol.* **2008**, *105*, 272–279. [CrossRef]
10. Salgado, U.D.; Weiß, C.; Michelic, S.K.; Bernhard, C. Fluid force-induced detachment criteria for nonmetallic inclusions adhered to a refractory/molten steel interface. *Metall. Mater. Trans. B* **2018**, *49*, 1632–1643. [CrossRef]
11. Lee, J.H.; Kang, M.H.; Kim, S.K.; Kim, J.H.; Kim, M.S.; Kang, Y.B. Influence of Al/Ti Ratio in Ti-ULC steel and refractory components of submerged entry nozzle on formation of clogging deposits. *ISIJ Int.* **2019**, *59*, 749–758. [CrossRef]
12. Bernhard, C.; Xia, G.; Karasangabo, A.; Egger, M.; Pissenberger, A. Investigating the influence of Ti and P on the clogging of ULC steels in the continuous casting process. In Proceedings of the 7th European Continuous Casting Conference, Duesseldorf, Germany, 27 June 2011.
13. Kimura, H. Advances in High-Purity IF Steel Manufacturing Technology. *Nippon. Steel Tech. Rep.* **1994**, *61*, 65–69.
14. Basu, S.; Chouahary, S.K.; Girase, N.U. Nozzle clogging behaviour of Ti-bearing Al-killed ultra low carbon steel. *ISIJ Int.* **2004**, *44*, 1653–1660. [CrossRef]
15. Lyons, C.; Kaushik, P. Inclusion characterization of titanium stabilized ultra low carbon steels: Impact of oxygen activity before deoxidation. *Steel Res. Int.* **2011**, *82*, 1394–1403. [CrossRef]
16. Gao, S.; Wang, M.; Guo, J.L.; Wang, H.; Zhi, J.G.; Bao, Y.P. Characterization transformation of inclusions using rare earth Ce treatment on Al-killed titanium alloyed interstitial free steel. *Steel Res. Int.* **2019**, *10*, 1900194. [CrossRef]
17. Gao, S.; Wang, M.; Guo, J.L.; Wang, H.; Zhi, J.G.; Bao, Y.P. Extraction, distribution, and precipitation mechanism of TiN–MnS complex inclusions in Al-killed titanium alloyed interstitial free steel. *Met. Mater. Int.* **2021**, *27*, 1306–1314. [CrossRef]
18. Yuan, B.H.; Liu, J.H.; Zhou, H.L.; Huang, J.H.; Zhang, S.; Shen, Z.P. Refining effect of IF steel produced by RH forced and natural decarburization process. *Chin. J. Eng.* **2021**, *43*, 1107–1115.
19. Dorrer, P.; Michelic, S.K.; Bernhard, C.; Penz, A.; Rössler, R. Study on the influence of FeTi-addition on the inclusion population in Ti-stabilized ULC steels and its consequences for SEN-clogging. *Steel Res. Int.* **2019**, *90*, 1800635. [CrossRef]
20. Park, D.C.; Jung, I.H.; Rhee, P.C.H.; Lee, H.G. Reoxidation of Al–Ti containing steels by CaO–Al_2O_3–MgO–SiO_2 slag. *ISIJ Int.* **2004**, *44*, 1669–1678. [CrossRef]
21. Jiang, M.F.; Zhang, Z.X.; Wang, D.Y.; Liu, J. Inclusions in characteristics of Ti/Al deoxidation steel and the analysis of nozzle clogging problem. *Ind. Heat.* **2011**, *40*, 60–63.
22. Deng, X.X.; Ji, C.X.; Cui, Y.; Tian, Z.H.; Yin, X.; Shao, X.J.; Yang, Y.D.; Mclean, A. Formation and evolution of macro inclusions in IF steels during continuous casting. *Ironmak. Steelmak.* **2017**, *44*, 739–749. [CrossRef]
23. Yang, W.; Li, S.S.; Li, Y.B.; Wang, X.H.; Zhang, L.F.; Liu, X.F.; Shan, Q.L. Evolution of inclusions in Ti-bearing ultra-low carbon steels during RH refining process. *Mater. Pro. Fund.* **2013**, 3–16. [CrossRef]
24. Wang, C.; Nuhfer, N.T.; Sridhar, S. Transient behavior of inclusion chemistry, shape, and structure in Fe-Al-Ti-O melts: Effect of gradual increase in Ti. *Metall. Mater. Trans. B* **2010**, *41*, 1084–1094. [CrossRef]
25. Bai, X.F.; Sun, Y.H.; Zhang, Y.M. Transient evolution of inclusions during Al and Ti additions in Fe-20 mass pct Cr alloy. *Metals* **2019**, *9*, 702. [CrossRef]
26. Yang, W.; Zhang, Y.; Zhang, L.F.; Duan, H.J.; Wang, L. Population evolution od oxide inclusions in Ti-stabilized ultra-low carbon steels after deoxidation. *J. Iron Steel Res.* **2015**, *22*, 1069–1077. [CrossRef]
27. Wang, M.; Bao, Y.P.; Cui, H.; Wu, H.J.; Wu, W.S. The composition and morphology evolution of oxide inclusions in Ti-bearing ultra low-carbon steel melt refined in the RH process. *ISIJ Int.* **2010**, *50*, 1606–1611. [CrossRef]
28. Doo, W.C.; Kim, D.Y.; Kang, S.C.; Yi, K.W. The morphology of Al-Ti-O complex oxide inclusions formed in an ultra low-carbon steel melt during the RH process. *Met. Mater. Int.* **2007**, *13*, 249–255. [CrossRef]
29. Qin, Y.M.; Wang, X.H.; Huang, F.X.; Ji, C.X. Behavior of non-metallic inclusions of IF steel during production process. *J. Northeast Univ. (Nat. Sci.)* **2015**, *36*, 1614–1618.
30. Sun, M.K.; Jung, I.-H.; Lee, H.-G. Morphology and Chemistry of Oxide inclusions after Al and Ti complex deoxidation. *Met. Mater. Int.* **2008**, *14*, 791–798. [CrossRef]
31. Marie-Aline, V.E.; Guo, M.X.; Zinngrebe, E.; Dekkers, R.; Proost, J.; Blanpain, B.; Wollants, P. Morphology and growth of alumina inclusions in Fe–Al alloys at low oxygen partial pressure. *Ironmak. Steelmak.* **2009**, *36*, 201–208. [CrossRef]
32. Jin, Y.; Liu, Z.Z.; Takata, R. Nucleation and growth of alumina inclusion in early stages of deoxidation: Numerical modeling. *ISIJ Int.* **2010**, *50*, 371–379. [CrossRef]
33. Van Ende, M.-A.; Guo, M.X.; Proost, J.; Blanpain, B.; Wollants, P. Formation and Morphology of Al_2O_3 inclusions at the onset of liquid Fe deoxidation by Al addition. *ISIJ Int.* **2011**, *51*, 27–34. [CrossRef]

34. Yang, G.W.; Wang, X.H.; Huang, F.X.; Wang, W.J.; Yin, Y.Q. Transient inclusion evolution during RH degassing. *Steel Res. Int.* **2014**, *85*, 26–34. [CrossRef]
35. Wakoh, M.; Sano, N. Behavior of alumina inclusions just after deoxidation. *ISIJ Int.* **2007**, *47*, 627–632. [CrossRef]